Available online at www.sciencedirect.com

SciVerse ScienceDirect

Ceramics International 39 (2013) 3563–3568

CERAMICS INTERNATIONAL

www.elsevier.com/locate/ceramint

Structural and ferroelectric properties of chemical solution deposited (Nd, Cu) co-doped $BiFeO_3$ thin film

C.M. Raghavan, J.W. Kim, S.S. Kim*

Department of Physics, Changwon National University, Changwon, Geongnam 641-773, Republic of Korea

Received 18 September 2012; received in revised form 9 October 2012; accepted 9 October 2012
Available online 17 October 2012

Abstract

Effects of (Nd, Cu) co-doping on the structural, electrical and ferroelectric properties of $BiFeO_3$ polycrystalline thin film have been studied. Pure and co-doped thin films were prepared on $Pt(111)/Ti/SiO_2/Si(100)$ substrates by using a chemical solution deposition method. Significant improvements in the electrical and the ferroelectric properties were observed for the co-doped thin film. The remnant polarization ($2P_r$) and the coercive field ($2E_c$) of the co-doped thin film were 106 μC/cm^2 and 1032 kV/cm at an applied electric field of 1000 kV/cm, respectively. The improved properties of the co-doped thin film could be attributed to stabilized perovskite structures, reduced oxygen vacancies and modified microstructures.

Keywords: A. Films; A. Sol–gel processes; B. X-ray methods; C. Ferroelectric properties

1. Introduction

Multiferroic bismuth ferrite $BiFeO_3$ (BFO) has been intensively studied and also projected for the replacement of toxic lead zirconium titanate in integrated microelectronic memory devices due to its large remnant polarization [1–3]. Formation of the stable single phase, low crystallization temperature and high Curie ($T_c \sim 1103$ K) and Néel ($T_N \sim 643$ K) transition temperatures are major advantages of the BFO compared to other perovskite multiferroic materials [3].

There are many techniques established for the fabrication of the BFO thin films [4]. Among these techniques, a sol–gel based chemical solution deposition (CSD) method is uncomplicated to achieve homogeneous thin film over large area, with easy-to-maintain stoichiometry, and low processing temperature [5]. However, the BFO thin film fabricated via a CSD method attains easy electrical breakdown and difficulties were found in measuring the saturated ferroelectric hysteresis loop due to large leakage current density [2,6,7]. The large leakage current density in the BFO thin film is believed to mainly originate from oxygen vacancies, volatilization of Bi ions, valence fluctuation of Fe^{3+} ions (Fe^{2+}/Fe^{3+}), impurity phases and poor microstructures [8,9]. There are immense ongoing researches to control the leakage current density and to improve the ferroelectric properties of the BFO thin film via different approaches, such as use of single crystal substrates, forming resistive buffer layers, construction of multilayer structures, making solid solutions and cationic substitution [10].

Inclusion of impurities into Bi- and Fe-sites of the BFO using rare earth (Eu, La, Nd, Gd, Sm, Ho, etc.) and transition metal (Ni, Cr, Ti, Mn, Sc, etc.) ions has been strongly suggested to control the factors which cause large leakage current density and to improve the ferroelectric properties of the BFO [11,12]. The rare earth ions doped into Bi-sites stabilize the perovskite structure, retain the non-centrosymmetry and control the vaporization of Bi ions [9,13,14]. The transition metal ions at Fe-sites reduce the valence fluctuation of Fe^{3+} ions and fill oxygen vacancies based on the valence compensation [9].

There are limited studies on rare earth and transition metal ions co-doped BFO thin films. It is important to investigate the effects of co-doping elements on the improvements of electrical and multiferroic properties of the BFO thin film.

*Corresponding author. Tel.: +82 552133421; fax: +82 552670264.
E-mail address: sskim@changwon.ac.kr (S.S. Kim).

0272-8842/$ - see front matter © 2012 Elsevier Ltd and Techna Group S.r.l. All rights reserved.
http://dx.doi.org/10.1016/j.ceramint.2012.10.182

In this study, effects of (Nd, Cu) co-doping on the structure and the electrical properties, such as leakage current, dielectric and ferroelectric properties, were investigated and the results are discussed in detail.

2. Experimental procedure

All chemicals were purchased from Aldrich and used for the precursor solution preparation without further purification. The raw materials used for the precursor solutions were bismuth nitrate pentahydrate ($Bi(NO_3)_3 \cdot 5H_2O$) (99.99%), iron nitrate nonahydrate ($Fe(NO_3)_3 \cdot 9H_2O$) (99.99%), neodymium nitrate hexahydrate ($Nd(NO_3)_2 \cdot 6H_2O$) (99.999%) and copper nitrate hemi-hydrate ($Cu(NO_3)_2 \cdot 2.5H_2O$) (99.99%). Initially, 2-methoxyethanol (99.9%) and ethylene glycol (99.99%) were mixed together by constant stirring at 40 °C in a water bath for 30 min and used as a solvent. Bismuth nitrate pentahydrate (5 mol% excess) was added to the mixed solvent and stirred for 30 min. To the above Bi-solution acetic acid (99.99%) was added to make a weak acid medium and to catalyze the reaction and stirred for 30 min in turn. Finally, iron nitrate nonahydrate was added to form the BFO precursor solution. The resulting solution was subjected to continuous stirring for 3 h at room temperature. For the doping experiment, before the addition of iron nitrate nonahydrate, a measured quantity of neodymium nitrate hexahydrate was added separately, copper nitrate hemi-hydrate was added to this and stirred for 30 min in turn. The resulting mixture was stirred for 3 h at room temperature. The concentration of all final solutions was adjusted to 0.1 M.

All thin films were deposited on Pt(111)/Ti/SiO_2/Si(100) substrates (Inostek, Korea) by using a spin coating method at a constant spinning rate of 3000 rpm for 20 s. After spin coating, the wet thin films were prebaked at 360 °C for 10 min on a hot plate. The coating and the prebaking were repeated 12 times to obtain the desired film thickness. Finally, all thin films were annealed at 550 °C for 30 min by using a conventional annealing process under a nitrogen atmosphere for crystallization.

In order to measure electrical properties, Pt electrodes (with areas of 1.54×10^{-4} cm^2) were deposited on the top surface of the thin films by ion sputtering through a metal shadow mask to form a capacitor structure. The structures of the thin films were investigated by using an X-ray diffractometer (Rigaku, MiniFlex II) and a Raman spectroscope (Jasco, NRS-3100). Surface morphologies and film thicknesses were analyzed by using a field emission scanning electron microscope (Tescan, MIRA II LMH). The ferroelectric hysteresis loops of the thin films were measured at a frequency of 10 kHz with triangular pulses by using a standardized ferroelectric test system (Modified Sawyer-Tower circuit with oscilloscope). The leakage current densities of the thin films were measured by using an electrometer (Keithley, 6517A). The dielectric properties of the thin films were studied by using an LF impedance phase analyzer (HP, 4192A).

3. Results and discussion

The X-ray diffraction (XRD) patterns of the pure $BiFeO_3$ (BFO) and the $Bi_{0.9}Nd_{0.1}Fe_{0.975}Cu_{0.025}O_{3-\delta}$ (BNFC) thin films deposited on Pt(111)/Ti/SiO_2/Si(100) substrates are shown in Fig. 1(a). Both the thin films were indexed with reference to the perovskite BFO structure [JCPDS No. 72-2035]. The randomly oriented rhombohedral perovskite structure has been observed for the thin films. There were no additional peaks for the secondary or impurity phases. However, for the co-doped thin film, small changes in the diffraction patterns corresponding to (100) and (100)/(1$\bar{1}$0) planes were observed. From the magnified XRD patterns (Fig. 1(b) and (c)), a slightly higher angle shift in the peak position at the 2θ values of 22.5° (100) and 32° (100)/(1$\bar{1}$0) was clearly observed in the BNFC thin film. This indicates changes in the lattice parameters of the BNFC thin film. Furthermore, the diffraction peaks corresponding to (100)/(1$\bar{1}$0) planes were clearly separated for the pure BFO thin film while the peaks were broad in the co-doped BNFC thin film (Fig. 1(c)). This broadening indicates distortion in the rhombohedral lattice of the BNFC thin film due to the internal chemical pressure induced by the co-doping elements [12]. The distortion caused by the doping elements has large influence on the polarization of the BFO based thin film [12,15].

The specific site of rare earth and transition metal ions in the BFO was investigated by using Raman scattering spectra. Fig. 2 shows Raman scattering spectra for the pure BFO and the co-doped BNFC thin films. According to the group theoretical calculation, there are 13 ($4A_1+9E$) fundamental active modes estimated for the rhombohedrally distorted space group $R3c$ [16]. All of the major active modes that appeared in the pure BFO and the co-doped thin films are in good agreement with those for the rhombohedrally distorted ($R3c$) perovskite structure. By fitting the measured spectra and

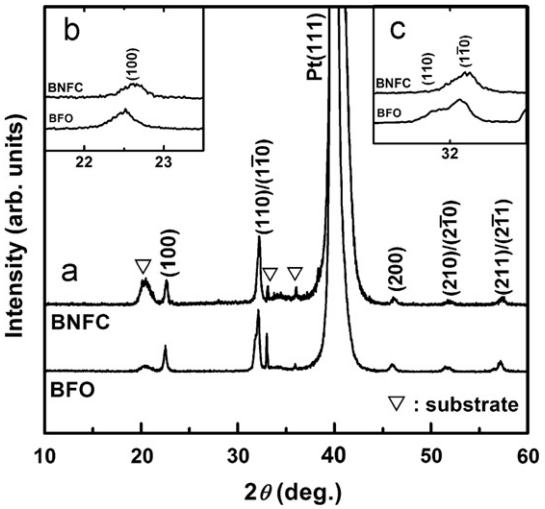

Fig. 1. XRD patterns of the BFO and the BNFC thin films deposited on Pt(111)/Ti/SiO_2/Si(100) substrates. Magnified XRD patterns in the vicinities of (a) 2θ=22.5° corresponding to (100) and (b) 2θ=32.0° corresponding to (110)/(1$\bar{1}$0) planes.

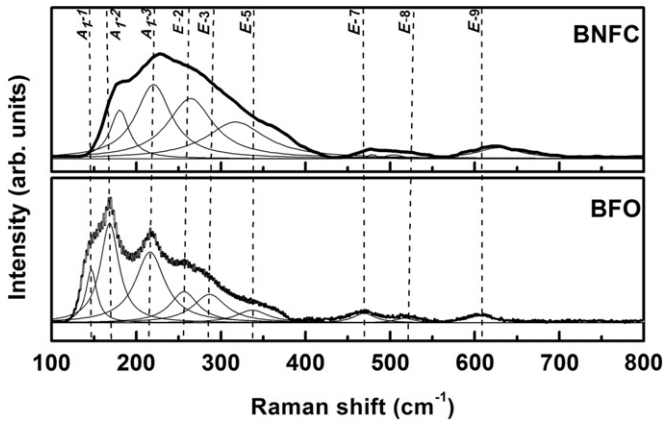

Fig. 2. Raman scattering spectra with fitted curves (thick solid lines) and the decomposed active modes (thin solid lines) of the BFO and the BNFC thin films.

Table 1
Assignment and comparison of the observed Raman frequencies of the BFO and the BNFC thin films.

Raman active modes	A_1-1	A_1-2	A_1-3	E-2	E-3	E-5	E-7	E-8	E-9
BFO (cm^{-1})	147	168	216	259	287	337	469	517	607
BNFC (cm^{-1})	154	169	227	257	273	335	476	520	619

decomposing the fitted curves into individual Lorentz components, the peak positions have been obtained. The Raman modes observed in the low frequency region are mainly related to the Bi–O vibration and the high frequency E modes are related to the Fe–O vibration [16,17]. As shown in Fig. 2, for the BNFC thin film, changes in peak intensity and peak broadening were observed at low frequencies. These are attributed to the dispersion of the Bi–O bonding by doping of rare earth Nd^{3+} ion for Bi sites [18]. The small shift in the peak positions at high frequencies for the co-doped BNFC thin film might be related to the Cu dopants on the Fe sites [19]. All observed Raman active modes for the pure BFO and the BNFC thin films are given in Table 1.

The surface morphologies of the thin films are shown in Fig. 3. From the top view of the SEM images, change in the surface morphology has been clearly observed for the co-doped thin film compared to the pure BFO thin film. Inclusion of the Nd^{3+} and the Cu^{2+} ions into the BFO was observed to increase the grain size and reduce the grain boundary. However, non-uniformity in the size distribution of the grains was observed in the BNFC thin film compared to the pure BFO thin film. The formation of non-uniform grain size for the BNFC thin film might be attributed to the variant distribution of Nd^{3+} and Cu^{2+} in the BFO matrix. Similar microstructural features have already been observed for the (La, Ni) co-doped BFO thin film [2]. The variation in the film thicknesses of the pure and co-doped thin films is represented in the cross sectional images.

Fig. 4(a) shows leakage current densities (J) as functions of applied electric field (E) for the pure BFO and the BNFC

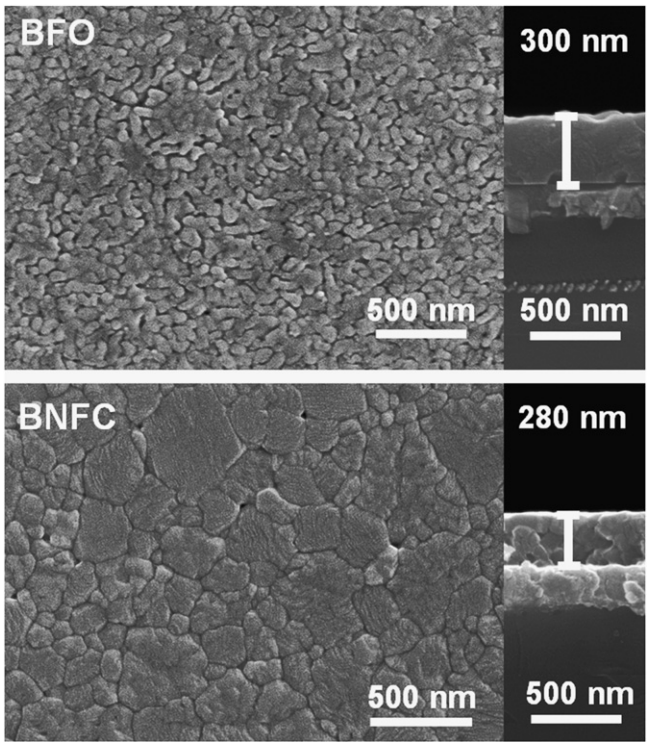

Fig. 3. SEM images of the surface morphologies and cross-sectional views of the BFO and the BNFC thin films.

thin films. From the leakage current density analysis, the J value of the BNFC thin film was three orders lower than that of the pure BFO thin film. The measured leakage current density of the BFO thin film at an applied electric field of 100 kV/cm was 2.58×10^{-2} A/cm^2. At the same applied electric field, the leakage current density for the BNFC thin film was 1.15×10^{-5} A/cm^2. The reduced leakage current density in the co-doped BNFC thin film could be associated with the decrease of oxygen vacancies, the control of valence fluctuation of Fe^{3+} ions and the improved microstructure by the Nd and Cu co-doping elements [20]. It is well documented that the presence of small amount of rare earth ions at Bi sites suppresses volatilization of Bi ions and stabilizes the perovskite structure [9,13]. The high bond dissociation energy of the Nd–O bond (703 ± 34 kJ/mol) compared to that of the Bi–O bond (343 ± 6 kJ/mol) controls the volatilization of Bi ions and stabilizes the perovskite structure [9]. Doping of divalent Cu^{2+} ion obstructs the formation of Fe^{2+} ions and controls the Fe^{2+}/Fe^{3+} charge fluctuation [8], but favors the formation of oxygen vacancies [13]. The possible mechanism for the formation of oxygen vacancies by Cu^{2+} ions at Fe-sites could be described using Kröger–Vink notations as follows:

$$2CuO \rightarrow 2Cu'_{Fe} + O_O^{\times} + V_O^{\bullet\bullet},$$

where $V_O^{\bullet\bullet}$ represents the oxygen vacancy with two positive charges and $O_O^{\times}$ represents the null charge on oxygen. That is, when two Fe^{3+} ions are substituted by two Cu^{2+} ions, oxygen vacancy with two positive charges is

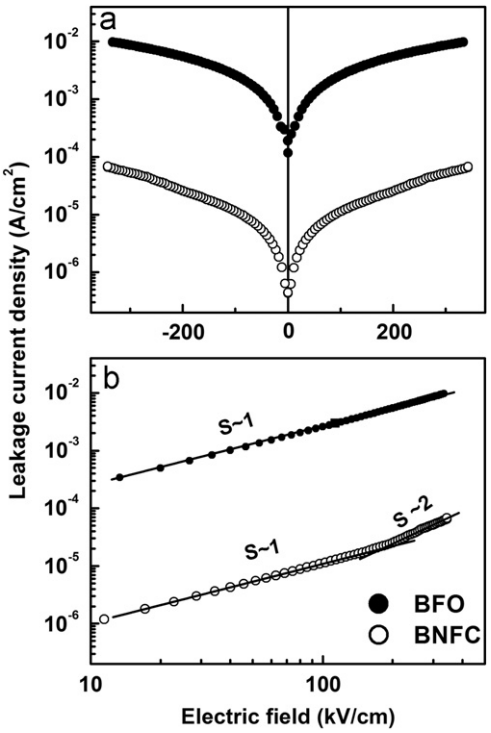

Fig. 4. (a) Leakage current densities of the BFO and the BNFC thin films measured at room temperature and (b) log (J)–log (E) characteristics of each film showing the conduction mechanisms.

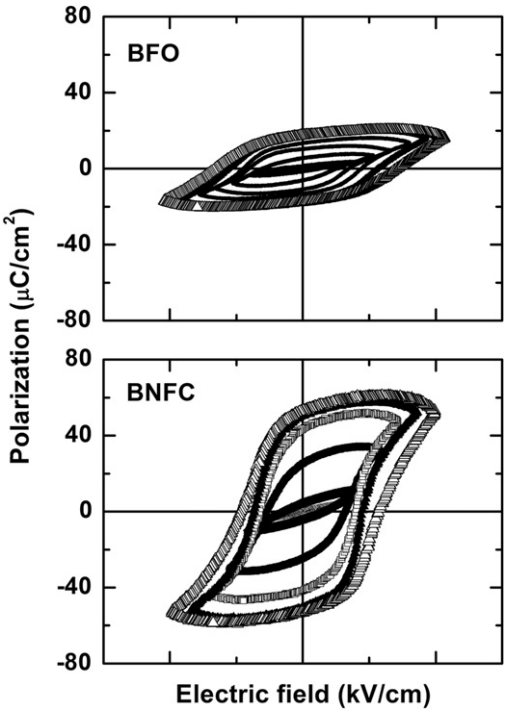

Fig. 5. Ferroelectric P–E hysteresis loops of the BFO and the BNFC thin films measured at room temperature at 10 kHz frequency.

introduced to maintain the charge neutrality [13]. The oxygen vacancy can form a defect dipole with $2Cu'_{Fe}$ as $[2Cu'_{Fe}-V_O^{\bullet\bullet}]^{\times}$ [21]. Thus, the dipoles formed by the charge compensation may lead to the decrease of leakage current density and the increase of polarization in the BFO thin film [21]. In the perovskite octahedra, different positions of oxygen vacancy lead to different electrostatic attractions between the defect carriers in the $[2Cu'_{Fe}-V_O^{\bullet\bullet}]^{\times}$ dipoles. This means that different electrical fields is required to break the dipole and to form the corresponding charge carriers [21].

The leakage current mechanism was analyzed using logarithmic plot of leakage current density versus applied electric field (log(J)–log(E)) as shown in Fig. 4(b). For the pure BFO thin film, the linear slope ($S\sim1$) over the entire region of applied electric field indicates Ohmic conduction mechanism [22]. The co-doped BNFC thin film showed Ohmic conduction ($S\sim1$) mechanism in the low electric field region, which is dominated by thermally stimulated free electrons. However, at high electric fields, the slope value was observed to be $S\sim2$, indicating a change in the conduction mechanism from Ohmic conduction to space charge limited conduction [22]. This indicates that the density of free electrons due to carrier injection becomes greater than the density of thermally stimulated electrons [23].

The ferroelectric polarization–electric field (P–E) hysteresis loops for the thin films are shown in Fig. 5. From the hysteresis loop analysis, the co-doped BNFC thin film shows improved ferroelectric properties, such as large remnant polarization ($2P_r$) and low coercive field ($2E_c$), compared to the pure BFO thin film. The measured $2P_r$ and $2E_c$ values of the BFO and the BNFC thin films were 35.2 μC/cm^2 and 1363 kV/cm (at 1068 kV/cm) and 106 μC/cm^2 and 1032 kV/cm (at 1000 kV/cm), respectively. The poor ferroelectric properties observed in the pure BFO thin film are attributed to the large leakage current density [8]. The formation of oxygen vacancies and the charge fluctuation of Fe^{3+} (Fe^{2+}/Fe^{3+}) in the perovskite structure are unfavorable for the polarization switching, leading to the decrease of P_r value [24]. Moreover, large grain boundary with small grains also results in low P_r and large leakage current in the pure BFO thin film. The increase of remnant polarization and the decrease of coercive field in the BNFC thin film are well correlated with the decrease of leakage current density and the lattice distortion caused by the co-doping elements [12]. Fig. 6 shows the variation of $2P_r$ and $2E_c$ as functions of applied electric field. The values of $2P_r$ and $2E_c$ increase with the increase of applied electric field. In addition, the $2P_r$ values for the BNFC thin film are well saturated compared to those of the pure BFO thin film.

Frequency dependent dielectric properties for the BFO and the BNFC thin films were measured at room temperature by varying the frequencies from 100 Hz to 1 MHz. As shown in Fig. 7, the dielectric constants of the thin films gradually decrease with the increase of frequency. The dielectric constants of the BFO and the BNFC thin films were 121 and 140 respectively, at an applied frequency of 1 kHz. At the same frequency, the measured dielectric losses for the pure BFO and the BNFC thin films were 0.049 and 0.038, respectively. The high

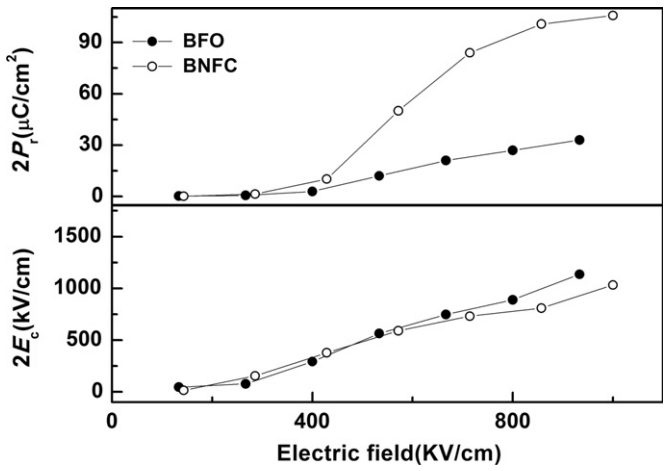

Fig. 6. Variations of $2P_r$ and $2E_c$ as functions of applied electric field of the BFO and the BNFC thin films.

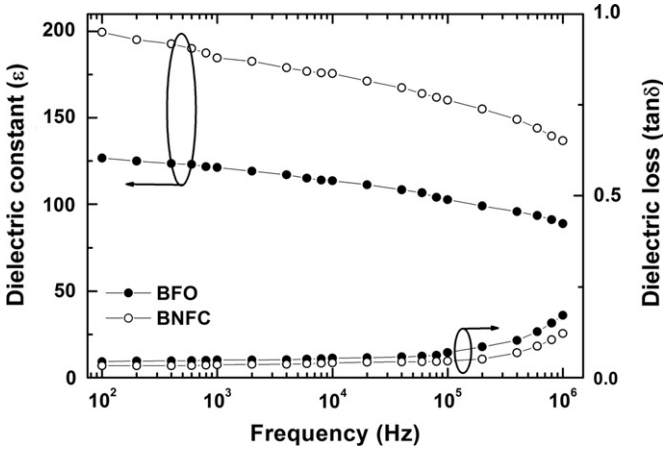

Fig. 7. Dielectric constants and dielectric losses as functions of frequency of the BFO and the BNFC thin films.

dielectric constant and the low dielectric loss of the BNFC thin film are correlated with the large remnant polarization and the low leakage current density.

4. Conclusions

Effects of (Nd, Cu) co-doping on the structural, electrical and ferroelectric properties of the BFO thin films prepared on Pt(111)/Ti/SiO_2/Si(100) substrates via a chemical solution deposition were investigated. The distorted rhombohedral perovskite structures for the pure BFO and the co-doped thin films were confirmed by using XRD and Raman scattering analysis. Significant improvements, such as reduced leakage current density and increased remnant polarization, were observed for the co-doped thin film. The leakage current density of the co-doped thin film was three orders lower than that of the pure BFO thin film. It is concluded that the (Nd, Cu) co-doping into BFO leads to dense microstructure, decreasing of leakage current and saturated hysteresis loop with large polarization and low coercive field.

Acknowledgment

This work was supported by Priority Research Centers Program through the National Research Foundation of Korea (NRF) funded by the Ministry of Education, Science and Technology (2010-0029634).

References

[1] A.H.M. Gonzalez, A.Z. Simões, L.S. Cavalcante, E. Longo, J.A. Varela, C.S. Riccardi, Soft chemical deposition of $BiFeO_3$ multiferroic thin films, Applied Physics Letters 90 (2007) 052906.
[2] S.K. Singh, K. Maruyama, H. Ishiwara, Reduced leakage current in La and Ni co-doped $BiFeO_3$ thin films, Applied Physics Letters 91 (2007) 112913.
[3] V.R. Singh, A. Garg, D.C. Agrawal, Structural changes in chemical solution deposited lanthanum doped bismuth ferrite thin films, Applied Physics Letters 92 (2008) 152905.
[4] L. Hongri, S. Yuxia, Substantially enhanced ferroelectricity in Ti doped $BiFeO_3$ films, Journal of Physics D: Applied Physics 40 (2007) 7530–7533.
[5] R.W. Schwartz, T. Schneller, R. Waser, Chemical solution deposition of electronic oxide films, Comptes Rendus Chimie **7** (2004) 433–461.
[6] Y.P. Wang, L. Zhou, M.F. Zhang, X.Y. Chen, J.M. Liu, Z.G. Liu, Room-temperature saturated ferroelectric polarization in $BiFeO_3$ ceramics synthesized by rapid liquid phase sintering, Applied Physics Letters 84 (2004) 1731–1733.
[7] J.K. Kim, S.S. Kim, W.–J. Kim, A.S. Bhalla, R. Guo, Enhanced ferroelectric properties of Cr-doped $BiFeO_3$ thin films grown by chemical solution deposition, Applied Physics Letters 88 (2006) 132901.
[8] X.D. Qi, J. Dho, R. Tomov, M.G. Blamire, J.L.M. Driscoll, Greatly reduced leakage current and conduction mechanism in aliovalent-ion-doped $BiFeO_3$, Applied Physics Letters 86 (2005) 062903.
[9] Z. Hu, M. Li, Y. Yu, J. Liu, L. Pei, J. Wang, X. Liu, B. Yu, X. Zhao, Effects of Nd and high-valence Mn co-doping on the electrical and magnetic properties of multiferroic $BiFeO_3$ ceramics, Solid State Communications 150 (2010) 1088–1091.
[10] J. Wu, G. Kang, J. Wang, Electrical behavior and oxygen vacancies in $BiFeO_3/[(Bi_{1/2}Na_{1/2})_{0.94}Ba_{0.06}]TiO_3$ thin film, Applied Physics Letters 95 (2009) 192901.
[11] A. Lahmar, S. Habouti, M. Dietze, C.-H. Solterbeck, M. Es-Souni, Effects of rare earth manganites on structural, ferroelectric, and magnetic properties of $BiFeO_3$ thin films, Applied Physics Letters 94 (2009) 012903.
[12] F. Yan, M. Lai, L. Lu, T.J. Zhu, Enhanced multiferroic properties and valence effect of Ru-doped $BiFeO_3$ thin films, Journal of Physical Chemistry C 114 (2010) 6994–6998.
[13] Q. Ke, X. Lou, Y. Wang, J. Wang, Oxygen-vacancy-related relaxation and scaling behaviors of $Bi_{0.9}La_{0.1}Fe_{0.98}Mg_{0.02}O_3$ ferroelectric thin films, Physical Review B 82 (2010) 024102.
[14] V.R. Singh, A. Garg, D.C. Agrawal, Structural changes in chemical solution deposited lanthanum doped bismuth ferrite thin films, Applied Physics Letters 92 (2008) 152905.
[15] D. Rout, K.-S. Moon, S.L. Kang, Temperature-dependent Raman scattering studies of polycrystalline $BiFeO_3$ bulk ceramics, Journal of Raman Spectroscopy 40 (2009) 618–626.
[16] H.M. Tütüncü, G.P. Srivastava, Electronic structure and zone-center phonon modes in multiferroic bulk $BiFeO_3$, Journal of Applied Physics 103 (2008) 083712.
[17] P. Hermet, M. Goffinet, J. Kreisel, Ph. Ghosez, Raman and infrared spectra of multiferroic bismuth ferrite from first principles, Physical Review B 75 (2007) 220102R.

[18] N. Jeon, D. Rout, I.W. Kim, S.J. Kang, Enhanced multiferroic properties of single-phase $BiFeO_3$ bulk ceramics by Ho-doping, Applied Physics Letters 98 (2011) 072901.
[19] A.Z. Simões, R.F. Pianno, E.C. Aguiar, E. Longo, J.A. Varela, Effect of niobium dopant on fatigue characteristics of $BiFeO_3$ thin films grown on Pt electrodes, Journal of Alloys and Compounds 479 (2009) 274–279.
[20] S.K. Sing, H. Ishiwara, K. Sato, K. Maruyama, Microstructure and frequency dependent electrical properties of Mn-substituted $BiFeO_3$ thin films, Journal of Applied Physics 102 (2007) 094109.
[21] G.D. Hu, S.H. Fan, C.H. Yang, W.B. Wu, Low leakage current and enhanced ferroelectric properties of Ti and Zn co-doped $BiFeO_3$ thin film, Applied Physics Letters 92 (2008) 192905.
[22] J. Wu, J. Wang, D. Xiao, J. Zhu, Leakage mechanism of cation-modified $BiFeO_3$ thin film, AIP Advances 1 (2011) 022138.
[23] B.T. Phan, C. Jung, T. Choi, J. Lee, Trap-controlled space-charge-limited current conduction in the Cr-doped $SrTiO_3$ thin films deposited by using pulsed laser deposition, Journal of Korean Physical Society 51 (2007) 664–668.
[24] G.L. Yuan, S.W. Or, H.L.W. Chan, Z.G. Liu, Reduced ferroelectric coercivity in multiferroic $Bi_{0.825}Nd_{0.175}FeO_3$ thin film, Journal of Applied Physics 101 (2007) 024106.